Mixing and available potential energy in stratified flows

Yu-heng Tseng[a] and Joel H. Ferziger
Environmental Fluid Mechanics Laboratory, Stanford University, Stanford, California 94305-4020

(Received 14 July 2000; accepted 1 February 2001)

Mixing plays an important role in atmospheric and oceanic flows. It occurs on the small scales, is due to molecular diffusion, and is irreversible. On the other hand, stirring is a kinematic process that enhances mixing but is reversible. Budgets of the available potential energy, which require that the reference potential energy be computed, are used to study these processes. We develop an approach for calculating the available potential energy from the probability density function that is more efficient than existing methods, especially in two and three dimensions. It is suitable for application to both numerical simulations and experiments. A new length scale is defined which quantifies stirring and provides a measure of the strength of overturns resulting from stirring as well as their size. Simulations of lid-driven cavity flow and stratified homogeneous turbulent shear flow provide illustrations of the method. The new length scale is similar to Thorpe scale in lid-driven cavity flow and closely related to the Ellison scale in homogeneous sheared turbulence. © *2001 American Institute of Physics.* [DOI: 10.1063/1.1358307]

I. INTRODUCTION

Mixing is an important process in density stratified geophysical flows. Energy is extracted from the mean flow through shear production of turbulence while buoyancy stabilizes the flow by converting vertical turbulent kinetic energy into available potential energy (APE) through stirring.[1–3] Which mixing mechanisms are active depends on the nature of the external forcing and the stratification. In the open ocean, many mechanisms have been identified. The surface shear stress induced by the wind produces a homogeneous well-mixed layer whose lower boundary is transported downward by entrainment. This situation can be reproduced in the laboratory using oscillating grids and simulated by direct numerical simulation.[4–6] Turbulent mixing can be created in the ocean by surface and internal wave breaking and by tidal forcing. Our objective in this study is to develop an approach to investigate turbulent mixing qualitatively based on the length scales and energy budgets.

A. Length scales in stratified flows

The strength of mixing in the ocean is partially determined by the length scales of the turbulent eddies.[2,7–9] The behavior of a stratified turbulent flow depends on a balance of three types of forces: inertial, buoyant, and viscous. Buoyancy forces act on the largest scales of vertical motion and tend to suppress them. Viscous forces act on the smallest scales and determine their size.

One important scale in the presence of buoyancy is the Ozmidov scale, $L_O=(\varepsilon/N^3)^{1/2}$ where ε is the kinetic energy dissipation rate and N is the Brunt–Väisälä frequency ($N=\sqrt{-(g/\overline{\rho})\partial\overline{\rho}/\partial z}$). L_O is the largest scale that can overturn so scales larger than L_O are dominated by buoyancy. However, overturning length scales greater than L_O can occur when internal waves are present.[6,10] Waves contribute to the overturning scale but not the Ozmidov scale.[1] If the vertical velocity fluctuations due to internal waves are small compared to those of turbulence, the buoyancy scale $L_B=(\overline{w^2})^{1/2}/N$ can be used instead of the Ozmidov scale.[2]

Ellison (1957)[11] proposed an overturning length scale defined by $L_E=-\rho_{\rm rms}/(\partial\overline{\rho}/\partial z)$ where $\rho_{\rm rms}$ is the root mean square (rms) density fluctuation. L_E is a typical vertical distance travelled by a fluid particle before beginning to return to its equilibrium level or mixing.

Another commonly used scale is the Thorpe scale, L_T;[12] it is obtained by reordering the density profile into a stable monotonic profile. Thorpe's method is useful when the sampled data is on a single vertical line or when the flow is horizontally homogeneous. Let the vertical density profile have N layers, the jth of which has density ρ_j and depth Z_j. If this layer must be moved to depth Z_k to generate a stable profile then its Thorpe displacement is $d_j=(Z_j-Z_k)$. Typically, these displacements are computed using a bubble sort. For large data sets, quicksort can be used instead. On average it is the fastest known sorting algorithm. An illustration of the sorting process is given in Fig. 1. The Thorpe scale L_T is defined as the rms of the displacements

$$L_T=(\overline{d_j^2})^{1/2}. \tag{1}$$

L_T is proportional to the mean eddy size provided that the horizontal density gradient is much smaller than the vertical gradient. Thus it is an overturning scale.

Thorpe displacements are useful in estimating vertical mixing.[13] Strongly mixing flows are characterized by large displacements that are negative at the top of the domain and positive at the bottom. The sorted state is a reference state of minimum potential energy (Fig. 1). A strong correlation between L_T and L_E is found in laboratory experiments and numerical simulations except at high Richardson number

[a]Author to whom correspondence should be addressed. Electronic mail: yhtseng@stanford.edu

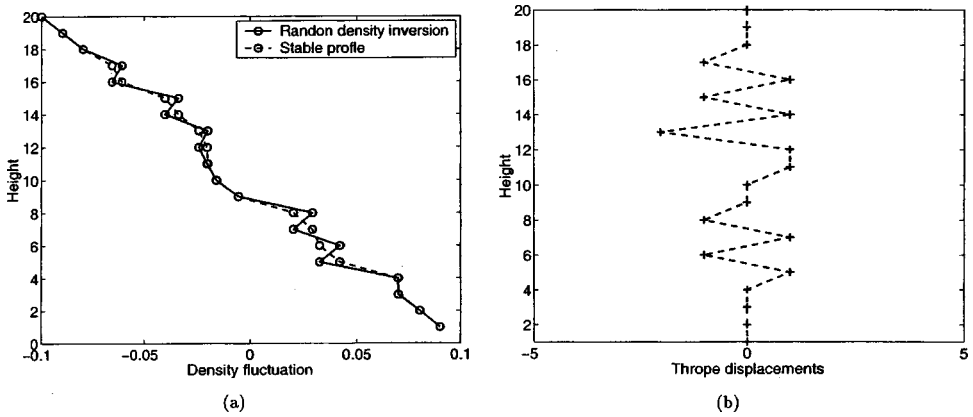

FIG. 1. (a) A hypothetical density inversion profile and the reordered stable density profile. (b) The corresponding Thorpe displacements.

(Ri).[2,7,14] Weak internal waves do not affect L_T but do affect L_E. Previous work indicates that L_T and L_O are linearly related when the flow is dominated by buoyancy.[7,13,15]

Winters *et al.*[3] gave a precise, three-dimensional (3D), mathematical sorting method. However, the definition of the Thorpe scale in three dimensions is ambiguous. Since L_T is computed by reordering each individual vertical density profile, most researchers define L_T in 3D as the rms of the one-dimensional (1D) Thorpe displacements.[2] One can also define a three-dimensional version of Thorpe scale, L_{T3D}, which is computed using the location, Z_* of the particle when horizontal as well as vertical displacements are allowed.[3] It is the rms of the vertical component of these displacements $(z(\mathbf{x},t)-Z_*(\mathbf{x},t))$ over the domain. L_T is a measure of vertical overturning only, while L_{T3D} is a measure of scalar displacements in general.[14] Internal waves may affect L_{T3D} but not L_T but, otherwise, the differences are usually small.

Inertial forces are balanced by viscous effects at the Kolmogorov scale, $L_K=(\nu^3/\varepsilon)^{1/4}$.

B. Mixing and stirring

Mixing and stirring are distinct processes. Stirring is a mechanical process that brings fluids of different densities into contact through the action of strain and vertical motion, thus converting kinetic energy into potential energy. After the fluid has been stirred, it may mix or re-stratify through gravitational settling. Mixing is the process of diffusion across interfaces to produce fluid of intermediate density and is an irreversible process.

The concepts of mixing and stirring have been studied by several groups.[16–18] However, accurate distinction between them in experiments is not easy. Aref and Jones[17] investigated reversible chaotic advection and irreversible diffusion via numerical experiments. Broadwell and Mungal[16] discussed scalar mixing in turbulent shear layers and jets using experimental results. They considered large-scale entrainment, stirring at the large scales, and diffusional mixing at the small scales. Diffusion acts over a longer interface in a stirred and stretched blob than in an unstirred one. On the other hand, Rehmann[18] applied scaling analysis to estimate mixing and investigated Schmidt number effects on the mixing efficiency in towed-grid turbulence experiments. If γ is the ratio of the mixing time to the decay time of the turbulence, little mixing occurs when $\gamma \gg 1$ as a stirred fluid parcel returns to its original position before the density difference can diffuse away. When $\gamma \ll 1$, a stirred parcel immediately loses its identity by mixing with the surrounding fluid. His scaling analysis of the effects of the Richardson, Reynolds, and Schmidt number agrees well with previous experiments.[9,16,18]

Many other observations show that molecular diffusion plays a non-negligible role in turbulent stratified flows.[9,19,20] However, there is disagreement on *how* the diffusivity affects turbulent mixing. Ivey and Imberger[9] suggested that molecular diffusivity plays a significant role when $\mathrm{Sc}<1$ and the density fluctuations are rapidly dissipated. Some laboratory experiments and numerical simulations support this hypothesis. According to Ivey and Imberger,[9] experimental results show a peak flux Richardson number, R_f, in air ($\mathrm{Sc}=0.7$) that is about 20% lower than that in saltwater ($\mathrm{Sc}=700$). Their measurements in heated water ($\mathrm{Sc}=7$) agree with the saltwater result. Itsweire and Helland (1989)[21] found that scales smaller than $3L_K$ do not contribute to the vertical mass flux. Other results suggest that diffusivity contributes to mixing greatly even when $\mathrm{Sc}>1$. Holt *et al.*[1] found that the vertical mass flux decreases from $\mathrm{Sc}=1$ to $\mathrm{Sc}=4$. Other researchers proposed a critical Peclet number ($\mathrm{Pe}=\mathrm{ReSc}$)[19] or a critical Richardson number Ri, which could depend on Pe and Sc.[22,23] The entrainment rate is thought to be dominated by the molecular diffusivity below a critical Pe or above a certain Ri. In addition to the Peclet number, Breidenthal (1992)[24] considered the effects of the Schmidt, Richardson, and Reynolds numbers on entrainment at stratified interfaces. The effect of molecular diffusivity is still not completely clear. In this study, we will explore the molecular diffusivity effect in lid-driven cavity flow and homogeneous sheared turbulence.

C. Potential energy budgets

Molecular diffusion causes irreversible diapycnal mixing, increasing the reference potential energy. The latter is the potential energy of a state created by allowing the stirred fluid to settle reversibly to its lowest potential energy state; it was first introduced by Lorenz.[25] The rate of increase of the

reference potential energy is a fraction $\eta<1$ of the rate of turbulent energy production and is called the mixing efficiency.

Available potential energy (APE) may contribute to oceanic or atmospheric circulation as it can be converted into kinetic energy. It is defined as the difference between the actual potential energy and the potential energy of the reference state. The relation between available potential energy and mixing has been investigated by many researchers.[3,26–28] Winters *et al.*[3] derived a dynamic evolution equation for the APE of a Boussinesq fluid. Their analysis carefully distinguishes the total potential energy and the reference potential energy and is useful for evaluating irreversible diapycnal mixing rates in turbulence simulations.

The purpose of this study is to develop a method for evaluating the available potential energy through a probability density function (pdf) approach and to quantify diabatic mixing and stirring in terms of the available potential energy. This leads to a natural relationship between the APE and a length scale. The pdf approach is an efficient method for evaluating the reference potential energy in both numerical simulations and experiments and can easily be extended to more complicated flows. The length scale defined below characterizes vertical overturns produced by stirring events.

The rest of the paper is organized as follows. Section II describes the new pdf approach for calculating the APE and defines the new length scale. Section III applies the pdf approach to 2D lid-driven cavity flow and studies the effects of the nondimensional parameters on it. Section IV investigates the new length scale in homogeneous sheared turbulence and relates it to other length scales. Finally, the results are summarized and discussed in Sec. V.

II. THE PDF APPROACH FOR ENERGETIC ANALYSIS

In this section, we introduce the basis for the pdf approach and the new length scale. This approach is related to the one presented by Winters *et al.*[3]

A. The pdf method

An important task in studying the energetics of oceanic circulation is the evaluation of the available potential energy (APE), the difference between the actual total potential energy (TPE) and the potential energy of a reference state (RPE). The reference state is the one with minimum potential energy that can be obtained through the adiabatic redistribution of the density:[3]

$$\mathrm{APE}=\mathrm{TPE}-\mathrm{RPE}. \tag{2}$$

APE represents the part of the potential energy that is available for conversion into kinetic energy during adiabatic readjustment. The total potential energy in a cylindrical domain of volume V is

$$\mathrm{TPE}=\int_V \rho g z\, dV, \tag{3}$$

where ρ is the density of the fluid and z is the vertical spatial coordinate. Note that $\rho=\rho(\mathbf{x},t)$.

We next relate APE to the pdf. Let $\tilde{\rho}$ be the independent density variable in probability sample space, $\rho\in[\rho_m,\rho_M]$, where ρ_m and ρ_M are the minimum and maximum values of the density. The probability of density ρ in the range between $\tilde{\rho}$ and $\tilde{\rho}+d\tilde{\rho}$ is $P(\tilde{\rho})d\tilde{\rho}$. $P(\tilde{\rho})$ may be defined in terms of the volume integral of a delta function

$$P(\tilde{\rho})\equiv\frac{1}{V}\int_V \delta(\tilde{\rho}-\rho)dV. \tag{4}$$

Let us define $Z_r(\rho)$ to be the height of fluid of density ρ in the minimum potential energy state and let dZ_r be the thickness of the layer containing fluid of density between $\tilde{\rho}$ and $\tilde{\rho}+d\tilde{\rho}$. We use the notation $Z_r(\rho)$ in order to distinguish the pdf reference state from the spatial reference state, $Z_*(\mathbf{x})$. If we assume that all fluid layers have the same horizontal surface area A, the volume occupied by this fluid is

$$A\,dZ_r|_\rho=VP(\tilde{\rho})d\tilde{\rho}|_\rho. \tag{5}$$

If the domain is not cylindrical, the horizontal cross section A is a function of the vertical coordinate. Note that $\tilde{\rho}$ is a dummy (independent) variable in probability space. The reference state profile $Z_r(\rho)$ can be obtained by integrating (5) over $\tilde{\rho}$:

$$Z_r(\rho)=H\int_\rho^{\rho_M} P(\tilde{\rho})d\tilde{\rho}, \tag{6}$$

where $H=V/A$ is the height of the domain. The RPE can be written as

$$\mathrm{RPE}=gA\int_0^H \rho Z_r(\rho)dZ_r. \tag{7}$$

We can express the reference density profile as a function of the reference coordinate Z_r, i.e., $\rho(Z_r)$. The reference potential energy then becomes

$$\mathrm{RPE}=gA\int_0^H \rho(Z_r)Z_r\,dZ_r. \tag{8}$$

The calculation of the APE thus consists of the following steps. The density field is scanned and the fluid in each control volume is put into a bin. At the end of the scan, the normalized number of control volumes in each bin gives the pdf. Equation (6) is then used to compute $Z_r(\rho)$. Finally, Eq. (7) gives the RPE. As the TPE can be computed during the scan, we have enough information to compute the APE. This process is much more efficient than the sorting process used by Ref. 3, especially in two and three dimensions. It is easily applied to field or laboratory data.

The extension of the pdf approach to an arbitrary domain with complex geometry is straightforward. $Z_r(\rho)$ can be obtained directly from

$$\int_0^{Z_r(\rho)} A(z)dz=V\int_\rho^{\rho_M} P(\tilde{\rho})d\tilde{\rho}, \tag{9}$$

where $A(z)$ is the horizontal section area instead of constant section area A.

In order to ensure accuracy in calculating the RPE, we employed an adaptive mesh in probability sample space,

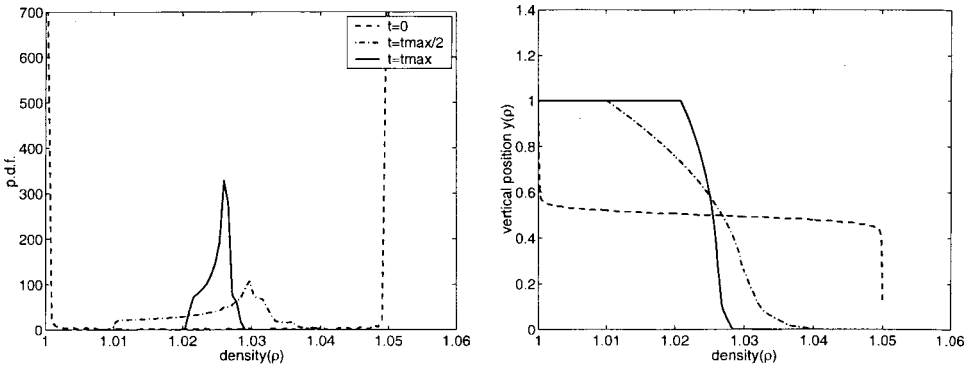

FIG. 2. (a) Typical pdf of density at the initial, intermediate, and final states of lid-driven cavity flow. (b) The reference state $y(\rho)$ at the initial $(--)$, intermediate $(-\cdot)$, and final $(—)$ states.

which allows for the possibility of delta functions in the initial density pdf, i.e., large amounts of fluid near the maximum and minimum densities [Fig. 2(a)]. Specifically, we use a Chebyshev transformation for discretizing the sample space instead of a uniform grid when the program detects a steep density gradient near the upper or lower bound of the probability space. When the probability is highly concentrated near ρ_M, the mesh near the boundary is chosen such that $x_j = dx\cos(\theta_j)$, $\theta_j = 0,\ldots,\pi/2$, and dx is the uniform mesh used in the other regions. Since it gives a finer grid near the boundaries, Chebyshev transformation is a good choice for discretizing the pdf.

B. Comparison with the existing approach

A method for calculating the APE was given by Dillon and Park[26] and Oort *et al.*[27] based on the quasigeostrophic approximation. Winters *et al.*[3] used the volume integral approach. In this section, we compare the current pdf approach with the common method developed by Winters *et al.*[3] for calculating the reference potential energy.

For the case of the constant horizontal section, the reference state height $Z_r(\rho)$ is the height of the water column times the cumulative pdf in space of $Z_*(\mathbf{x},t)$ defined in Ref. 3:

$$Z_*(\mathbf{x},t) = \frac{1}{A}\int_{V'} H(\rho(\mathbf{x}',t) - \rho(\mathbf{x},t))\,dV', \tag{10}$$

where H is the Heaviside step function

$$H(x) = \begin{cases} 0, & x<0, \\ \frac{1}{2}, & x=0, \\ 1, & x>0. \end{cases} \tag{11}$$

The most popular method of calculating the reference state Z_* is to sort the density field and interpolate it onto a fixed vertical grid. On the other hand, having the cumulative probability distribution, we can directly obtain spatial reference state, $Z_*(\mathbf{x},t)$, from $Z_r(\rho)$. Note that the spatial reference state is the vertical location in the sorted fluid occupied by a parcel found at $(\mathbf{x},t)$ in the unsorted fluid.

Let us compare the CPU-time required to calculate the reference potential energy by the pdf approach and the method of Winters *et al.*[3] in two-dimensional (2D) lid-driven cavity flow and 3D homogeneous sheared turbulence (Table I). The difference in the computed values of the RPE is $O(10^{-4})$ in lid-driven cavity flow and $O(10^{-3})$ in homogeneous turbulence and is primarily due to the discrete grid used in the pdf method (Fig. 3). The time is normalized by $T_c = \rho_0 U_{\text{lid}}^3/L_c$ in lid-driven cavity flow and dimensionless shear time S_t is used in homogeneous turbulence. When the grid count is large, the pdf analysis requires less calculation and is simpler to program. In calculating the reference state Z_* by the method of Winters *et al.*,[3] the CPU time is proportional to the total number of grid points in the physical domain (N^2 in two dimensions). For the computation by the pdf method, it depends only on how the pdf is discretized in probability density space. The savings are significant for large grids. The pdf approach is easily extended to the three-dimensional case as shown in Sec. IV and the computational cost savings are much larger (Table I).

C. Stirring length scale (L_S)

From the available potential energy defined above, a vertical stirring length scale L_S can be defined for a two-layer stratified fluid:

$$\frac{\text{APE}}{\rho_0 V} = g' L_S, \tag{12}$$

where $g' = g\Delta\rho/\rho_0$ is the reduced gravity and $\Delta\rho$ is the

TABLE I. Comparison of average CPU-time (10^{-1} s) for the RPE calculation.

Flow	Lid-driven cavity flow			Homogeneous turbulence
Platform	SunEnterprise 5500 (MATLAB)			Cray Y-MP (F90)
Grid size	32×32	64×64	80×80	128×128×128
Volume integration (Ref. 3)	1.35	15.60	37.66	176.66
Pdf approach	1.26	3.76	6.07	0.12

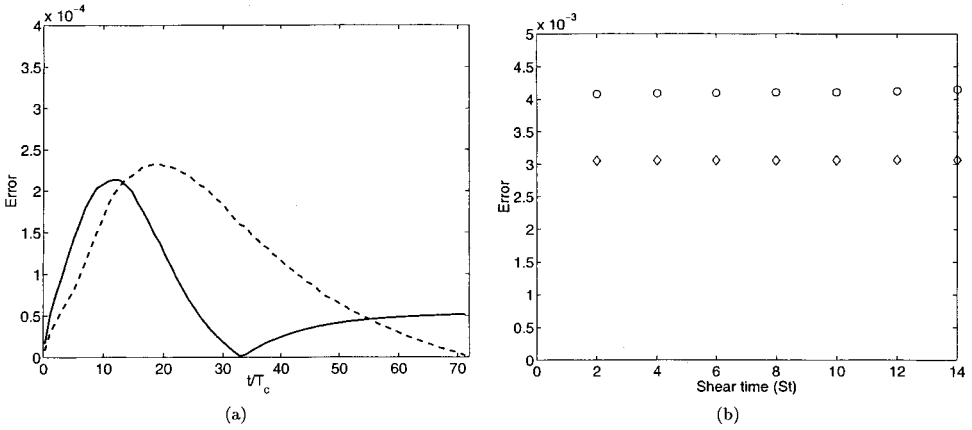

FIG. 3. The calculated difference between the reference potential energy computed via the pdf and sorting approaches (Ref. 3). (a) Lid-driven cavity simulations of Fig. 5 [−: case (a); −−: case (b)]. (b) Homogeneous sheared turbulence (◇: case px; ○: case fc).

difference between the maximum and minimum densities in the domain at any time. L_S can be regarded as a density weighted displacement.

In continuously stratified fluids, the expression for L_S can be rewritten in terms of the background buoyancy frequency N:

$$\frac{\mathrm{APE}}{\rho_0 V}=\frac{1}{2}N^2L_S^2, \quad L_S=\sqrt{\frac{2\mathrm{APE}}{\rho_0 V N^2}}. \tag{13}$$

The length scale L_S is clearly a measure of stirring and is affected by both overturning and the strength of the density fluctuations. In turbulent flows, the APE can be replaced by the fluctuating APE. L_S can be interpreted as the size of a turbulent patch generated by stirring but, as it is affected by the intensity of the density fluctuations, it is a kind of density weighted Thorpe scale. In the ocean, the stirring length scale usually cannot be measured directly and is usually approximated by the Thorpe scale.[26] The current energy budget analysis provides a way to fill this gap.

III. APPLICATION TO LID-DRIVEN CAVITY FLOWS

We shall use two flows to illustrate the pdf method for the available potential energy. First we consider initially stratified two-dimensional lid-driven flow in a square cavity. Then we shall look at homogeneous sheared stratified turbulence.

A. Numerical simulation of lid-driven flow

Lid-driven cavity flow is often used to test numerical methods. The governing equations for an incompressible, stratified flow are those of conservation of mass, momentum, and the density. The Boussinesq approximation is adopted:

$$\frac{\partial u_i}{\partial x_i}=0, \tag{14}$$

$$\frac{\partial}{\partial t}u_i+u_j\frac{\partial u_i}{\partial x_j}=-\frac{1}{\rho_0}\frac{\partial p}{\partial x_i}+\nu\frac{\partial^2 u_i}{\partial x_j\partial x_j}+\frac{\rho}{\rho_0}g_i, \tag{15}$$

$$\left(\frac{\partial}{\partial t}\rho+u_j\frac{\partial \rho}{\partial x_j}\right)=\alpha\frac{\partial^2\rho}{\partial x_j\partial x_j}. \tag{16}$$

These equations apply to both two- and three-dimensional flows, but we will consider only the two-dimensional case. The Reynolds number is

$$\mathrm{Re}=\frac{U_{\mathrm{lid}}L_c}{\nu}, \tag{17}$$

where $\rho=\rho_0+\rho'$, ρ_0 is the constant reference density, g_i is the gravity acceleration in the x_i direction, L_c is the width of the cavity, ν is the kinetic viscosity, and α is the molecular diffusivity.

The Schmidt number is

$$\mathrm{Sc}=\frac{\nu}{\alpha}. \tag{18}$$

A nonuniform Cartesian grid and a collocated arrangement for all of the variables is used[29] on a 128×128 grid.

The boundary conditions for the velocity are no-slip at all of the walls. In addition, no mass or heat flux is allowed at the walls. The lid velocity (U_{lid}) is constant and the initial velocity is zero in the cavity.[30] The velocity fields are obtained using the finite volume (FV) approach, the details of which are given in Hortmann *et al.*[29] and Ferziger and Perić.[31]

The density transport equation is discretized using a finite difference (FD) approach and solved using an approximate factorization scheme. We apply the Crank–Nicolson method for time advancement and second order central differencing in space. The scheme is unconditionally stable, but large time steps may produce oscillations so we use a time step of $O(10^{-2})$. The initial density field is a two-layer stratified flow with the density profile

$$\rho(z)=\overline{\rho}+\frac{\Delta\rho}{2}\frac{\mathrm{erf}((16\pi)^{1/2}(z-z_{1/2}))}{\mathrm{erf}((2\pi)^{1/2})}, \tag{19}$$

where $z_{1/2}$ is the vertical midpoint and $\overline{\rho}$ is the mean density. Typical density contours are shown in Fig. 4 for $\mathrm{Re}=2\times10^3$ and $\mathrm{Sc}=0.5$.

B. Energy budgets

We apply the pdf method to the lid-driven cavity flow. Figure 5 shows the evolution of the total potential energy,

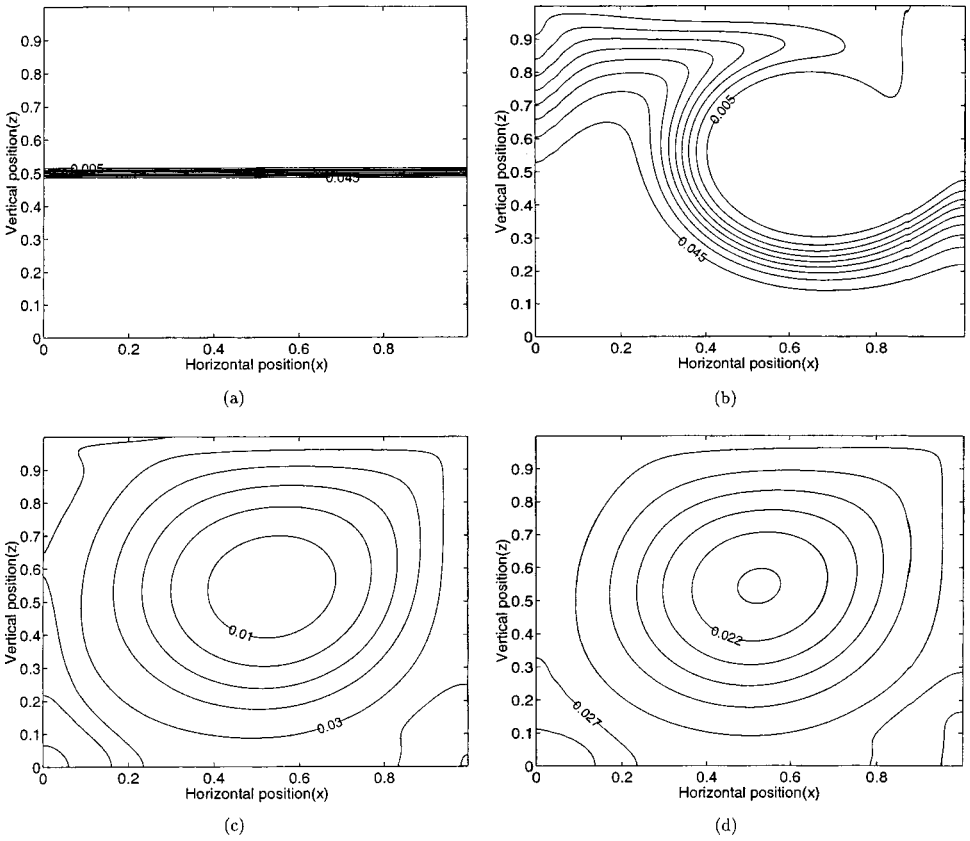

FIG. 4. Density contours for lid-driven simulation at $\mathrm{Re}=2\times10^3$, $\mathrm{Sc}=0.5$. (a) $t/T_c=0$, (b) $t/T_c=8$, (c) $t/T_c=24$, (d) $t/T_c=48$.

reference potential energy, and available potential energy for $\mathrm{Re}=1\times10^3$ and 2×10^3; $\mathrm{Sc}=1$ in both cases. As expected, the available potential energy is larger in the higher Reynolds number case due to more energetic stirring. The APE and TPE are almost equal at small times ($t/T_c<7$ for $\mathrm{Re}=1\times10^3$ and $t/T_c<10$ for $\mathrm{Re}=2\times10^3$) because there has not been enough time for mixing to occur. In the final steady state, most of the potential energy is in the form of RPE, i.e., the fluid is almost completely mixed.

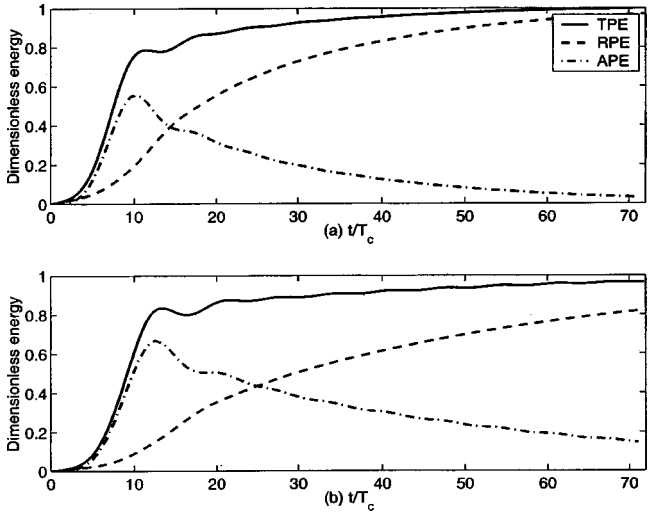

FIG. 5. Time evolution of the TPE, RPE, and APE for $\mathrm{Sc}=1$. (a) $\mathrm{Re}=1\times10^3$, (b) $\mathrm{Re}=2\times10^3$.

The pdfs of the initial and evolved states for $\mathrm{Re}=2\times10^3$ are shown in Fig. 2(a). The reference potential energy states $Z_r(\rho)$ are shown in Fig. 2(b).

Winters *et al.*[3] derived the dynamic equations for total potential energy and reference potential energy for a Boussinesq fluid. The former is

$$\frac{d}{dt}\mathrm{TPE}=-\int\int_S gx_3\rho u_i n_i\,ds+\alpha\int\int_S gz\frac{\partial\rho}{\partial x_i}n_i\,ds+\int\int_V\int g\rho u_3\,dV-\alpha\int\int_A g(\rho_u-\rho_b)dA, \tag{20}$$

where ρ_u and ρ_b are the density on the top and bottom surfaces, respectively. The first term represents the contribution of the convective flux at the boundaries of the domain. The second term is due to the diffusive mass flux at the boundary. Both of these are zero in the cavity flow. The third term is the exchange between kinetic energy and potential energy due to the buoyancy flux (a reversible process). The fourth term is the rate of potential energy increase due to diapycnal mixing.

The evolution of reference potential energy is governed by

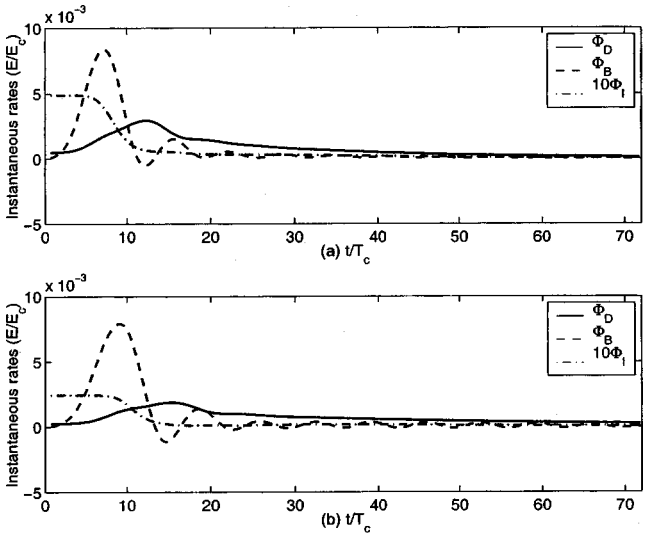

FIG. 6. The instantaneous rate of energy exchange. (a) Sc=1, Re=1 $\times 10^3$ and (b) Sc=1, Re=2×10^3.

$$\frac{d}{dt}\mathrm{RPE} = -\int\int_S g\left(\int^{\rho} Z_*(\rho')d\rho'\right) u_i n_i \, ds + \alpha\int\int_S g Z_* \frac{\partial \rho}{\partial x_i} n_i \, ds + \alpha\int\int_V\int g\left(-\frac{dZ_*}{d\rho}\right) \times \left|\frac{\partial \rho}{\partial x_i}\right|^2 dV, \tag{21}$$

Z_* is the reference state defined in Ref. 11. Since $\partial Z_*/\partial x_i = (dZ_*/d\rho)(\partial\rho/\partial x_i)$, the third term can be expressed in terms of $-dZ_*/d\rho$. The first two terms, which are the contributions of convective and diffusive transfer across the boundary, are zero in the cavity flow. The third term represents the rate of increase of the potential energy in the reference state due to mixing and is positive definite. An evolution equation for the pdf could also be derived. However, the resulting equation involves the time derivative of (6), leading to the occurrence of a conditional velocity at the boundary so a joint-pdf approach is needed to obtain a dynamic equation for the RPE. This will make the computation costly.[32]

The rate of change of the available potential energy is governed by

$$\frac{d}{dt}E_a = \frac{d}{dt}\mathrm{TPE} - \frac{d}{dt}\mathrm{RPE} = \int\int_V\int g\rho u_3 \, dV + \alpha\int\int_A g(\rho_b - \rho_u)\, ds - \alpha\int\int_V\int g\left(-\frac{dz_r}{d\rho}\right) \times \left|\frac{\partial \rho}{\partial x_i}\right|^2 dV = \Phi_B + \Phi_I - \Phi_D, \tag{22}$$

where the diapycnal mixing $\Phi_D = \alpha\int\int_V\int g\left(-dz_r/d\rho\right)\left|\partial\rho/\partial x_i\right|^2 dV$ is always positive. Φ_I is the second term of (22) and is the rate of conversion of kinetic energy to potential energy.[3,28] The contributions of the instantaneous rate of diapycnal mixing Φ_D, vertical buoyancy flux (Φ_B), and internal energy (Φ_I) to the APE are shown in Fig. 6. Before the densities at the top and the bottom begin to change, the contribution from diapycnal mixing (Φ_I) is con-

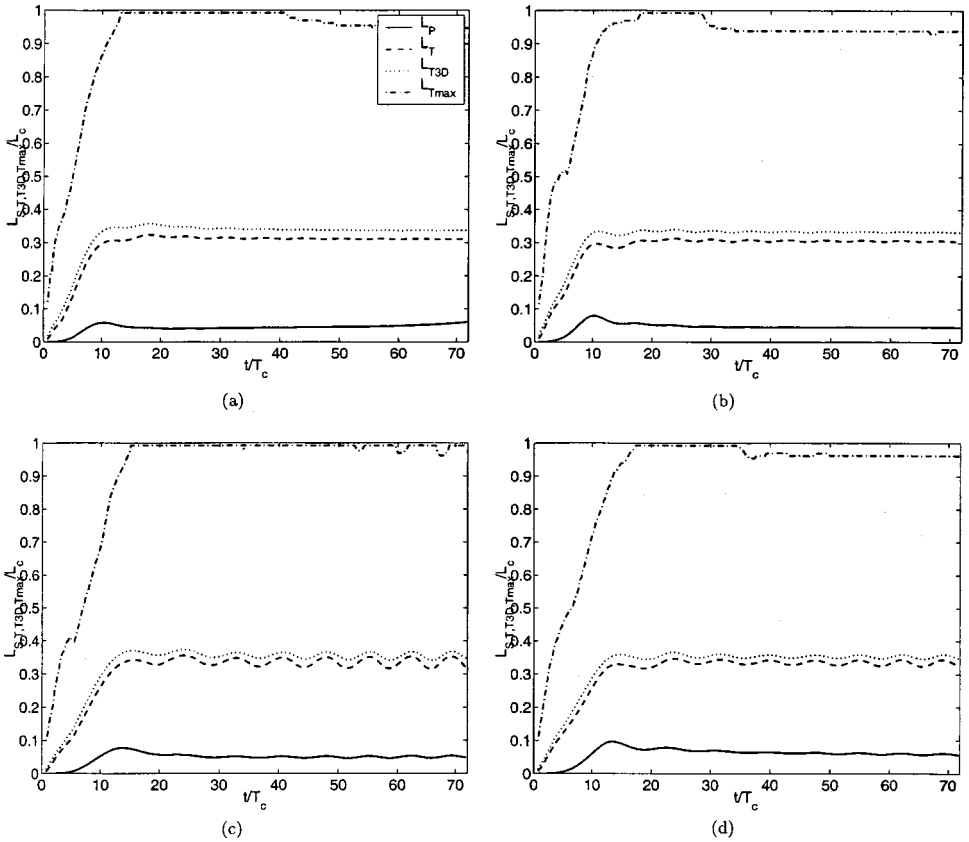

FIG. 7. Comparison of length scales L_S, L_T, $L_{T\,3D}$, and $L_{T\,\max}$ at (a) Sc =0.5, Re=1×10^3, (b) Sc=2, Re=1 $\times 10^3$, (c) Sc=0.5, Re=2.5×10^3, and (d) Sc=2, Re=2.5×10^3. $L_{T\,\max}$ is the maximum Thorpe displacement (–: L_S; – –: L_T; $\cdots$: $L_{T\,3D}$; $\cdot$–: $L_{T\,\max}$).

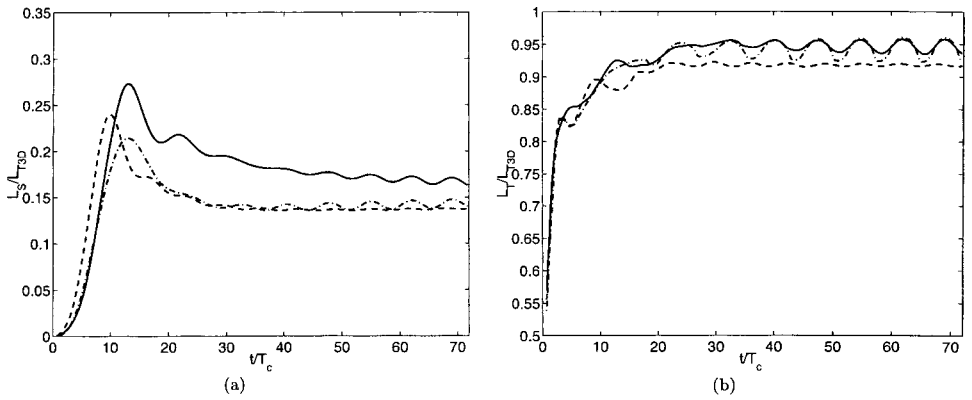

FIG. 8. The length scale ratio, $L_S/L_{T\,3D}$ (a) and $L_T/L_{T\,3D}$ (b), versus time. $--$: Sc=2, Re=1×10^3; $\cdot-$: Sc=0.5, Re=2.5×10^3; $-$: Sc=2, Re=2.5×10^3.

stant [for $t/T_c \leqslant 7$ in Fig. 6(a), $t/T_c \leqslant 9$ in Fig. 6(b)]. The exchange between kinetic energy and TPE, Φ_B, varies considerably. It is of the same magnitude as Φ_D initially and decreases as the flow evolves.

The diapycnal mixing rate, Φ_D, also increases substantially as expected [$t/T_c=0\sim13$ in Fig. 6(a), $t/T_c=0\sim17$ in Fig. 6(b)]. After some time, the buoyancy flux is nearly zero due to the disappearance of density fluctuations. However, diapycnal mixing continues and the RPE increases at all times.

C. Length scale and mixing efficiency in lid-driven cavity flow

Figure 7 compares the length scales L_S, L_T, $L_{T\,3D}$, and $L_{T\,\max}$ for various Schmidt and Reynolds numbers. The Thorpe scales (L_T and $L_{T\,3D}$) are defined in Sec. I and $L_{T\,\max}$ is the instantaneous maximum of L_T. L_S has a maximum at the same time as L_T. The higher Reynolds number cases [Figs. 7(c) and 7(d)] have larger fluctuations of the length scales due to more energetic stirring. L_S is larger at high Reynolds number [Figs. 7(c) and 7(d)] than at low Reynolds number [Figs. 7(a) and 7(b)], particularly at the first maximum while the Thorpe scales L_T and $L_{T\,3D}$, do not change appreciably with Re. L_T and $L_{T\,3D}$ are nearly equal in this flow as shown in Fig. 7.

L_S increases slightly with Schmidt number [Fig. 8(a)]. Since a smaller diffusivity cannot smooth out density differences as effectively, stronger density fluctuations occur at high Sc, i.e., there is more stirring. This is reflected in L_S but not in L_T. This does not necessarily imply higher mixing efficiency. The effect of molecular diffusion on mixing efficiency is discussed below.

Because it is density weighted, L_S quantifies stirring more reliably than L_T or $L_{T\,3D}$. The length scale ratio $L_S/L_{T\,3D}$ in Fig. 8(a) shows that there is more energetic stirring occurs at high Re and Sc. Figure 8(b) shows that the ratio of $L_T/L_{T\,3D}$ is very close to unity except during the initial transient. The deviation early on occurs because L_T is a measure of overturning while $L_{T\,3D}$ a better measure of stirring.[14]

The dependence of the maxima of L_S and $L_{T\,3D}$ on Re and Sc is presented in Figs. 9 and 10. Figure 9 shows that the maximum of L_S (lower lines) is roughly proportional to $\mathrm{Re}^{1/4}$ but the maximum of $L_{T\,3D}$ (upper lines) is almost indepen-

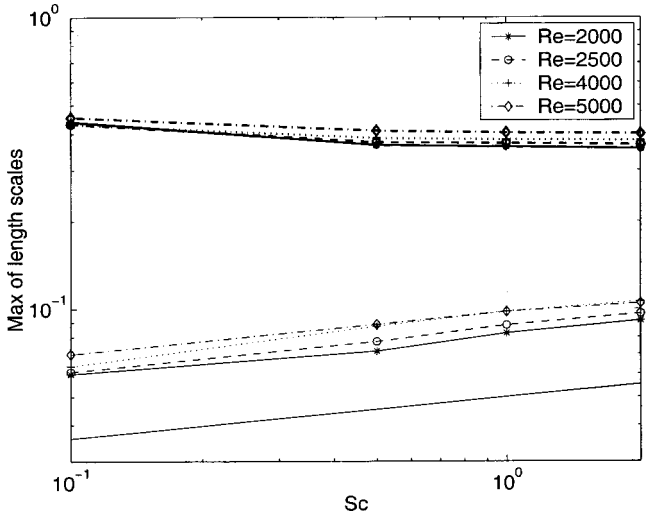

FIG. 9. The maximum Thorpe and stirring length scales versus Re at various Schmidt numbers. The upper bold lines denote maximum Thorpe scales and the lower lines denote the maximum stirring length scales. The lowest solid line has a slope of 1/4.

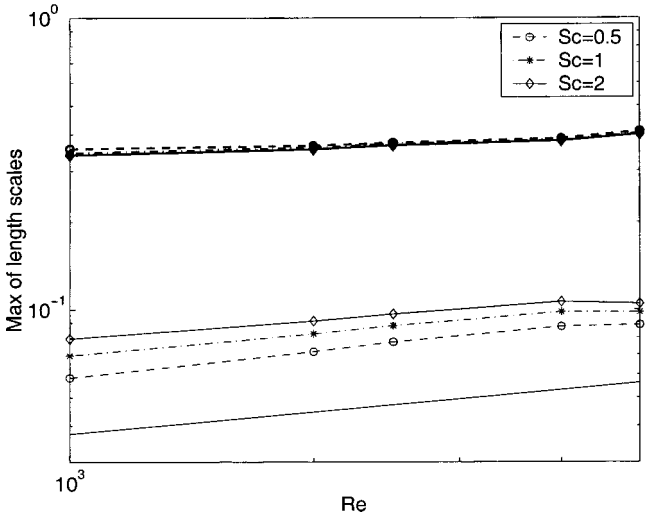

FIG. 10. The maximum Thorpe and stirring length scales versus Sc at various Reynolds numbers. The upper bold lines denote maximum Thorpe scales and the lower lines denote the maximum stirring length scales. The lowest solid line indicates slope 1/6.

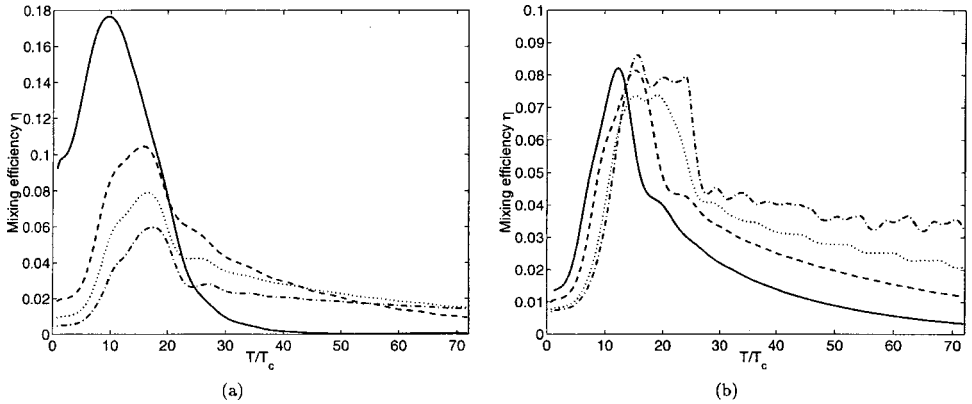

FIG. 11. The evolution of mixing efficiency for various values of Sc (–: Sc=0.1; – –: Sc=0.5; ···: Sc=1; ·–: Sc=2) at Re=2.5×10^3 (a) and different values of Re (–: Re=1×10^3; – –: Re=2×10^3; ···: Re=4×10^3; ·–: Re=5×10^3) at Sc=1. (b) The maximum mixing efficiency occurs immediately after the maximum overturns.

dent of Re. The behavior of L_S results from the greater available potential energy at high Re. The maximum of L_S is approximately proportional to $\mathrm{Sc}^{1/6}$. We do not want to overemphasize the significance of these results as they are for a laminar flow. However, the results do show that L_S quantifies stirring better than $L_{T\,3\mathrm{D}}$. Note that L_S is uniquely defined, as is $L_{T\,3\mathrm{D}}$, while the conventional Thorpe scale L_T may depend on the sampled locations.

Mixing in stratified flows is usually quantified by the down-gradient buoyancy flux. The mixing efficiency, η, is defined as the ratio of buoyancy flux to the energy available for mixing.[6,9] However, during transients or in the presence of counter-gradient fluxes, the mixing efficiency is better defined in terms of the irreversible mixing rate,[3] i.e., the portion of kinetic energy used to alter the reference potential energy. Thus the mixing efficiency is

$$\eta = \frac{\Delta \mathrm{RPE}}{\Delta \mathrm{KE}}, \tag{23}$$

where ΔRPE is the change in the reference potential energy and ΔKE is the kinetic energy input due to the top lid and is obtained by integrating the product of shear stress and lid velocity on the top. This definition gives a time-dependent mixing efficiency that satisfies $0 \leqslant \eta \leqslant 1$.

The effects of Schmidt and Reynolds numbers on the mixing efficiency in lid-driven cavity flow are demonstrated in Figs. 11(a) and 11(b). Figure 11(a) shows the mixing efficiency for different values of Sc at Re=2.5×10^3. The maximum mixing efficiency η_M increases as Sc decreases; in fact, $\eta_M \sim \mathrm{Sc}^{-1/2}$ (Fig. 12) as suggested by the following scaling analysis. For an individual fluid parcel, the mixing efficiency can be defined as the ratio of the mixed fluid volume to total volume. The mixed fluid volume changes due to diffusion. The mixing efficiency should be proportional to l/D where l is the diffusion length scale $[l \approx (\alpha t)^{1/2}]$ and D is the dimension of the parcel. Therefore, the mixing efficiency is proportional to the square root of molecular diffusivity α ($\mathrm{Sc}^{-1/2}$). These results are consistent with previous studies of low Reynolds number flow.[1,20] In the lid-driven cavity, the maximum mixing efficiency occurs just after the vertical length scales ($L_S, L_T, L_{T\,3\mathrm{D}}$) reach their maxima.

The effect of Reynolds number on the mixing efficiency is illustrated in Fig. 11(b). Figure 11(b) shows results for different values of Re at Sc=1. The maximum mixing efficiency does not depend significantly on Re. However, the Reynolds number does affect the mixing efficiency at longer times. Higher Re implies greater stirring and generation of a stronger vortex. The stronger vortex induces more mixing and the mixing event lasts longer [Fig. 11(b)].

IV. APPLICATION TO 3D STRATIFIED TURBULENCE

Homogeneous turbulence subjected to shear and stratification is the simplest flow in which most of the major phenomena found in geophysical turbulence occur. Thus, we apply the pdf approach to calculate its APE and compare the stirring scale (L_S) with other length scales.

A. Homogeneous sheared turbulence

There have been many studies of homogeneous stratified turbulence.[1,33–36] Rohr *et al.*[34] conducted laboratory experiments on this flow and found a stationary Richardson number $\mathrm{Ri}_s \approx 0.25$. The turbulent energy grows when $\mathrm{Ri} < \mathrm{Ri}_s$ (weak stratification) and decays when $\mathrm{Ri} > \mathrm{Ri}_s$ (strong stratification). As expected, Ri measures the relative effect of shear and buoyancy. The length scales L_O, L_E, and L_T are highly correlated with the turbulence intensity in homogeneous sheared turbulence.[2,34]

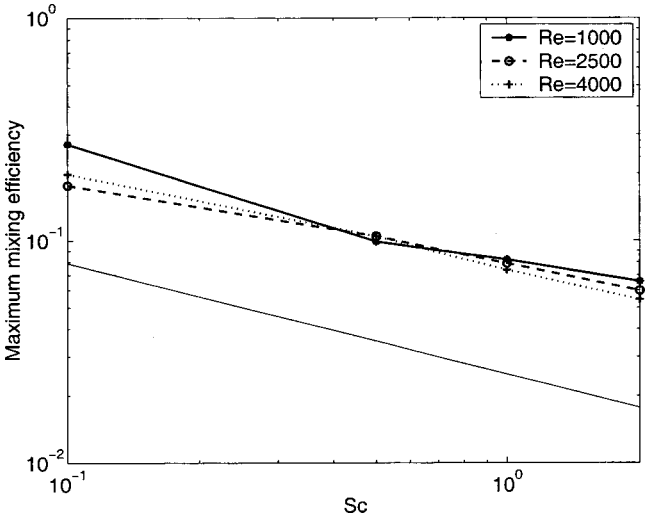

FIG. 12. Maximum mixing efficiency versus Sc at various Reynolds numbers. The solid line has slope −1/2.

Holt *et al.*[1] demonstrated the existence of a stationary Richardson number using direct numerical simulation, gave its dependence on Reynolds number, and suggested that its value is independent of the initial dimensionless shear rate and increases with increasing Re. Piccirillo and Van Atta[35] investigated the turbulence evolution in a homogeneous stratified shear flow using a thermally stratified wind tunnel and found a decrease of Ri_s with increasing grid size and thus increasing Reynolds number. Jacobitz *et al.*[36] performed numerical investigations to explain the apparently different dependence of Ri_s on the Reynolds number and proposed that in sheared and stratified homogeneous turbulence, the stationary Richardson number depends on both the Reynolds number and the initial dimensionless shear rate of the flow. Finally, a series of direct numerical simulations were performed by Shih *et al.*[37] over a range of initial Reynolds numbers (Re) and dimensionless shear rates (S^*). They found that the final shear rate $S^* \approx 11$ does not depend on initial shear rate at high Re and varies at low Re, in agreement with the results of Jacobitz *et al.*[36] Also, the dependence on Re is better correlated using a turbulent Froude number.[6,9,37]

B. Numerical simulations

In this study, we investigate the energy budgets and length scales in homogeneous stably stratified turbulent flow.[1,37] The governing equations are the same as those for lid-driven cavity flow [Eqs. (14), (15), and (16)]. However, the density is $\rho = \overline{\rho} + \rho'$ ($\overline{\rho} = \rho_0 + S_\rho x_3$), where $\overline{\rho}$ is the mean density and ρ' is the fluctuating density. The mean density is composed of a constant reference density ρ_0 and a specified mean density gradient (S_ρ is a constant), x_3 is the vertical coordinate. The velocity is decomposed as

$$u_i = \overline{U_i} + u_i', \tag{24}$$

where $\overline{U_i}$ is the mean velocity and u_i' is the fluctuating velocity. The mean velocity $\overline{U_i} = (Sx_3, 0, 0)$, where $S = dU_1/dx_3$ is the specified mean shear rate. The microscale Reynolds number is

$$\mathrm{Re}_\lambda = \frac{q\lambda_{11;1}}{\nu}, \tag{25}$$

where $\lambda_{11;1}$ is the Taylor microscale ($\lambda_{ij;k} = u_i'/u_{j,k}'$, where primes denotes root mean square quantities[1]) and q is the root mean square velocity.

The strength of the stratification is indicated by the gradient Richardson number

$$\mathrm{Ri} = \frac{N^2}{S^2} = \frac{-(g/\rho_0)S_\rho}{S^2}, \tag{26}$$

where $N = [-(g/\overline{\rho})(\partial\overline{\rho}/\partial z)]^{1/2}$ is the Brunt–Väisälä frequency. Ri is constant in each simulation. Other parameters are identical to those used previously. The gravitational acceleration is ($g = 980.7$ cm/s^2) and reference density ($\rho_0 = 1.006$ g/cm^3) are not varied in this study.

The code solves for the three-dimensional velocity and density fields using second order Runge–Kutta time advancement and periodic boundary conditions for all of the turbulent quantities. The scheme is based on the pseudospectral method developed by Rogallo *et al.*[38] A $128 \times 128 \times 128$ grid is used in this study and the stretching factors $\beta_1 = 0.63$ and $\beta_2 = \beta_3 = 1.26$ are used to map the physical domain onto a cubic box of length 2π, which allows for the shear-induced growth of the integral scales in the streamwise direction.[38] Details of the numerical method are given in Holt *et al.*[1] and Shih *et al.*[37] Aliasing error is avoided by using masking and random phase shifting.[38] This method results in a residual aliasing error of the same order as the error due to the time advancement scheme.

The initial energy spectrum is a k^2-exponential spectrum:[37]

$$E(k) = C\left(\frac{k}{k_p}\right)^2 e^{-2k/k_p}, \tag{27}$$

where C is a constant and k_p is the wave number at the peak of the spectrum. Shih *et al.*[37] showed that the results obtained with this initial spectrum are very similar to those obtained by Jacobitz *et al.*[36]

We shall investigate the effects of the Richardson, Reynolds, and Schmidt numbers. A reference case (case fc) is chosen; it is a stationary turbulence run of Shih *et al.*[37] with $\mathrm{Ri} = 0.16$, $\mathrm{Re}_\lambda = 89.4$, $Sc = 0.72$ and will be compared with other simulations. Shih *et al.*[37] suggested that the initial shear rate is significant at low Reynolds number. In order to include the influence of initial shear rate, the initial dimensionless shear rate, $S^* = Sq^2/\epsilon$, is 4 except in two low Reynolds number runs. The parameters of these simulations are summarized in Table II.

C. Characterization of the state of the turbulence and turbulent length scales

Active turbulence occurs at low Ri and is a state in which buoyancy forces are weak compared to inertial forces and do no prevent overturning and mixing. At high Ri, turbulence is suppressed by buoyancy on all scales. We are interested in the behavior of the stirring scale L_S and its comparison with other length scales in these flows.

It is well known that for $\mathrm{Ri} < \mathrm{Ri}_s$, L_O, L_E, and L_T grow when the flow is fully developed. Buoyancy controls the growth of the largest turbulent eddies. Active turbulence exists at the large scales.[1] For $\mathrm{Ri} > \mathrm{Ri}_s$, L_O, L_E, and L_T decrease as buoyancy suppresses the turbulent eddies. Countergradient fluxes may appear and internal waves become a significant component of the flow. Comparisons of the stirring, Thorpe, and Ellison scales are shown in Figs. 13 and 14. L_S, L_E, and $L_{T\,3\mathrm{D}}$ are all affected by internal waves.

TABLE II. Parameters of 3D homogeneous shear turbulence simulations.

Cases	bl	fc (stat.)	bp	px	pk	gc	gk	fx	fy
Ri	0.04	0.16	1.00	0.16	0.16	0.16	0.16	0.16	0.16
$\mathrm{Re}_{\lambda,\mathrm{initial}}$	89.4	89.4	89.4	22.4	22.4	44.7	44.7	89.4	89.4
Sc	0.72	0.72	0.72	0.72	0.72	0.72	0.72	0.1	4
S^*	4	4	4	4	8	4	8	4	4

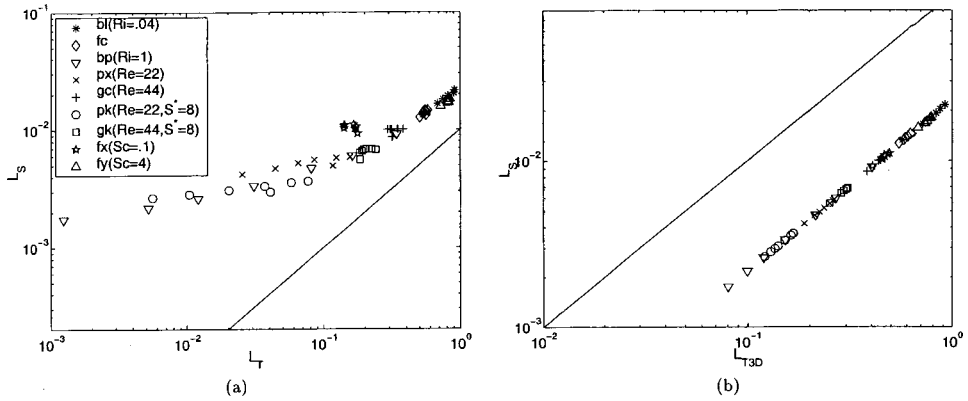

FIG. 13. Comparison of stirring scale (L_S) and the Thorpe scales [L_T (a) and $L_{T\,3D}$ (b)]. The solid line has slope unity.

Figure 13 compares the stirring and Thorpe scales (L_T and $L_{T\,3D}$). The scales are linearly related except at high Richardson number ($\mathrm{Ri}=1$) and low Reynolds number ($\mathrm{Re}_\lambda=22$). In the former case, internal wave motions contribute significantly to available potential energy, but do not affect L_T. Similarly, the Ellison (L_E) and Thorpe scales are closely related.[2] A high correlation between $L_{T\,3D}$ and L_E was observed in a Kelvin–Helmholtz instability simulation [compare Figs. 9(b) and 10(a) of Smyth and Moum (2000)[14]]. The correlation is easily demonstrated for a single overturning particle, but it is more difficult to explain in two and three dimensions. It is interesting to note that L_S is proportional to $L_{T\,3D}$, probably because the density fluctuations are the same (in a statistical sense) everywhere in the flow. Strong shear reduces both the stirring and Thorpe scales at low Reynolds number. The shear rate does not have a significant effect on the length scales.

The comparison of L_S and L_E is shown in Fig. 14. L_S is linearly correlated with L_E in all cases. That this should be so for homogeneous turbulence can be demonstrated as follows. Consider a particle whose density is greater than the reference density at its vertical position by $\delta\rho$. Then $(z-Z_*)$ can be approximated by $(\partial Z_*/\partial\rho)\delta\rho$. The fluctuating available potential energy (FAPE) is the volume integral of $\rho' g(z-Z_*)$ for the whole domain (ρ' is the density fluctuation) and can be related to L_E by

$$\begin{aligned}\mathrm{FAPE}&=\int_V \rho' g(z-Z_*)\,dV\\ &\approx\int_V \rho' g\left(\frac{\partial Z_*}{\partial\rho}d\rho\right)dV=\int_V g\frac{(\rho')^2}{\partial\overline{\rho}/\partial z}dV\\ &\approx gV\rho_{\mathrm{rms}}L_E,\end{aligned}\tag{28}$$

which shows that the fluctuating available potential energy is proportional to L_E and ρ_{rms}. Since $L_S=\sqrt{2\mathrm{FAPE}/\rho_0 VN^2}$, it is easy to show that the stirring scale L_S is proportional to $\sqrt{\rho' L_E/(\partial\overline{\rho}/\partial z)}=L_E$.

This result can also be explained by considering the available potential energy at a particular point in homogeneous turbulence. The FAPE can be correlated to L_E, i.e., $\mathrm{FAPE}=1/2\overline{\rho}N^2L_E^2$ (Refs. 1 and 39) so L_E is proportional to local $\sqrt{\mathrm{FAPE}/N^2}$. This indicates that L_E is a direct measure of fluctuating available potential energy.[2,33,39,40] However, L_E is a local quantity and may not be easy to compute accurately. On the other hand, the stirring scale (L_S) is a global quantity and is easily computed if the density field is known. Thus, L_S is a better indicator of the overall state of the flow than L_E. As already noted, L_S can be regarded as a density fluctuation weighted generalization of the Thorpe scale and is more similar to the 3D Thorpe scale than to the Ellison scale in many turbulent flows.

L_S can also be correlated with $\epsilon/\nu N^2$, a parameter often used in oceanic research to describe the state of the turbulence.[40,2] There is some disagreement as to the physical interpretation of this quantity. Some researchers refer to it as a buoyancy-based Reynolds number[2,14] while others refer to it as a small scale Froude number[8,9] and still others consider it a mixed parameter.[40] We believe that, because it contains both the viscosity and the buoyancy frequency, the last interpretation is to be preferred.

Active turbulence is supposed to be present only when $\epsilon/\nu N^2$ exceeds a certain critical value (≈ 20). We show the ratio L_S/L_I vs $\epsilon/\nu N^2$ in Fig. 15, where L_I is the integral scale of the turbulence and is defined as the average of the diagonal integral scales; i.e., $L_I=I_{ii,k}/3$, $I_{ij;k}=\int(\overline{u_i(x_m)u_j(x_m+r_k)})dr_k/(\overline{u_iu_j})$. All of the data lie in the active turbulence region (buoyancy-affected turbulence) ex-

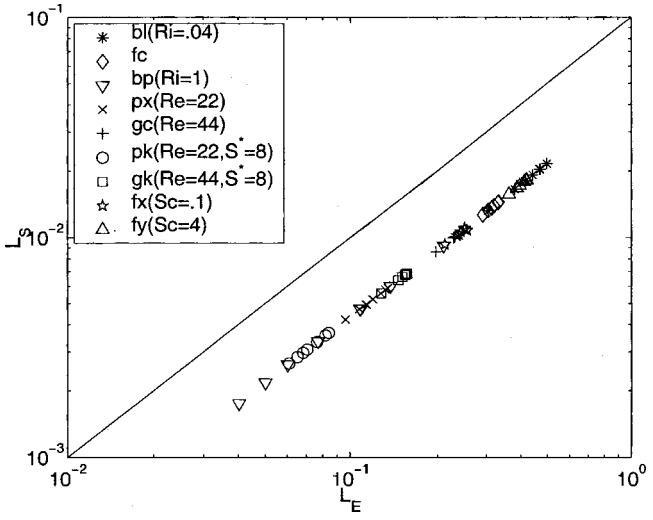

FIG. 14. Comparison of stirring scale (L_S) and Ellison scale (L_E). The solid line has slope unity.

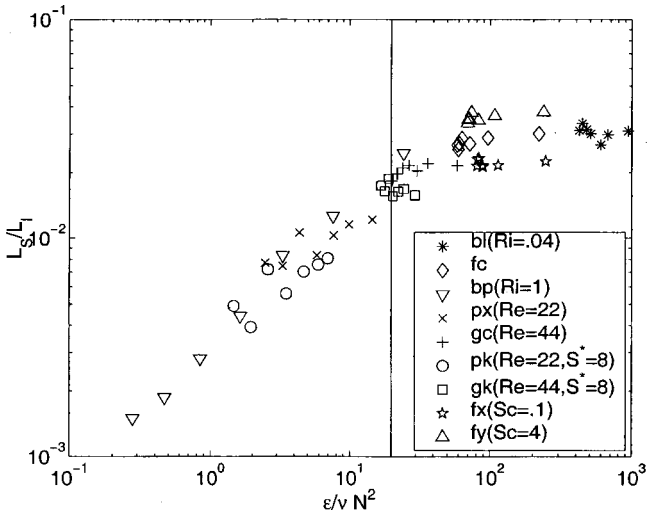

FIG. 15. The ratio of stirring and integral scales (L_S/L_I) vs $\epsilon/\nu N^2$. The solid line marks the onset of active and fossil turbulence.

cept those from the high Ri and low Re simulations in which the turbulence undergoes a transition from active to buoyancy dominated. Turbulence is completely suppressed in the high Ri simulation and L_S decays. Thus, L_S and L_I are comparable in the active turbulence region. In the transition from active to buoyancy-dominated turbulence there is an intermediate region in which there is a mix of active and fossil turbulence. The region was called buoyancy-controlled by Itsweire *et al.*[2] and, in it, the turbulence is not in equilibrium; in fact it decays. The onset of buoyancy control occurs at $\epsilon/\nu N^2 \approx 60$ according to Fig. 15. We thus see that the length scale (L_S) can be used as an indicator of the state of the turbulence. Finally, we note that L_S does not change significantly in stationary turbulence ($\mathrm{Ri}=\mathrm{Ri}_s$) and increases slightly as Sc increases (Fig. 15).

Figure 16 shows the ratios of L_S/L_B and L_S/L_O vs $\epsilon/\nu N^2$. The trends are similar since L_B and L_O are very close except in cases in which internal waves dominate so they can be used interchangeably as long as the turbulence is active. L_S and L_B are roughly equal when $\epsilon/\nu N^2 < 100$ at high Reynolds number, as has been shown in laboratory experiments and ocean measurements.[40] Since L_B represents the rms vertical distance that a particle with the rms kinetic energy can travel, it also is an indicator of the vertical kinetic energy of the turbulence.[39] On the other hand, L_S measures the available potential energy. Thus, L_B must be large before L_S can grow. Physically, kinetic energy is converted into potential energy until L_S and L_B are comparable. This point is referred to as a buoyancy-inertia transition by Gibson[41] and Yamazaki.[40] In low Re simulations, L_S departs from L_B at small $\epsilon/\nu N^2$ (the critical value of $\epsilon/\nu N^2$ is around 20 and 10 for $\mathrm{Re}=44$ and 22, respectively). The departures mark the beginning of buoyancy-controlled turbulence. The parameter $\epsilon/\nu N^2$ reflects the influence of Reynolds number and is thus a good correlation parameter (Fig. 16).

V. DISCUSSION AND CONCLUSIONS

In this study, we investigated energy budgets and mixing through the analysis of available potential energy. A probability density function approach was introduced and used to efficiently calculate the available potential energy. The pdf method is equally well suited for numerical and experimental determination of the APE and is more efficient than sorting methods. We also proposed a new length scale (L_S) that is a generalized density-fluctuation weighted Thorpe scale. This length scale has a clear physical interpretation and is a reliable parameter for gauging the strength of stirring. It is easy to obtain once the reference potential energy has been computed.

Lid-driven cavity flow and homogeneous sheared turbulence were used to illustrate the proposed method. More stirring occurs as Re increases but molecular diffusivity has little effect on it. The effect of Re on L_S is more significant than the effect of Sc, but the latter has a strong influence on mixing. Thus, Sc affects the mixing efficiency more than the Reynolds number does. The maximum mixing efficiency is proportional to $\mathrm{Sc}^{-1/2}$ in lid-driven cavity flow. The dependence on Re is mainly due to the enhancement of stirring.

In homogeneous sheared turbulence, the Richardson and Reynolds numbers are the important parameters. Higher Ri and lower Re reduce the stirring scale. As Sc increases, L_S increases. However, the effect is not as significant as it is in the lid-driven cavity flow. The new length scale (L_S) exhibits the same behavior as the Ellison and 3D Thorpe scales but is superior to those scales for characterizing the turbulent eddies because it is weighted with the density fluctuations. In addition, it is affected by internal waves and is a global mea-

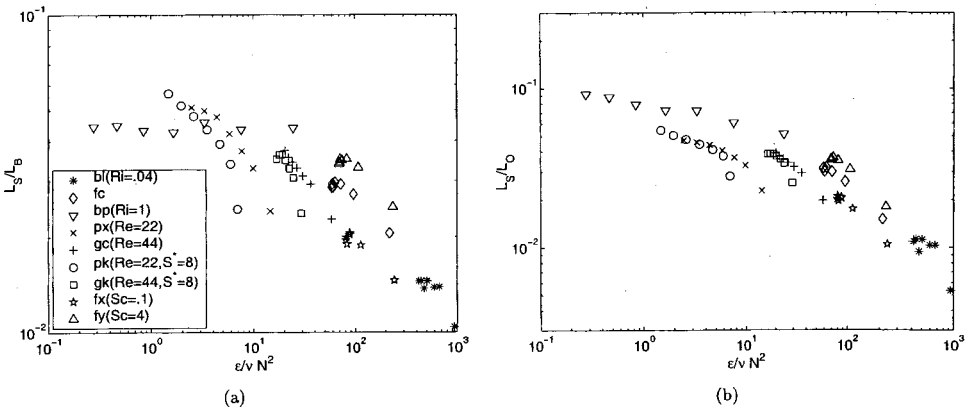

FIG. 16. (a) The ratio of stirring scale to buoyancy scale (L_S/L_B) vs $\epsilon/\nu N^2$. (b) The ratio of stirring scale to Ozmidov scale (L_S/L_O) vs $\epsilon/\nu N^2$.

sure of stirring rather than a local one like L_E. This length scale also provides a criterion for determining the state of turbulence. Comparison of these length scales in inhomogeneous flows is an interesting topic for further study.

ACKNOWLEDGMENTS

The authors thank Dr. Jeffrey Koseff for his helpful comments and Lucinda Shih for her invaluable help with the homogeneous turbulence simulation. Financial support for this work was provided by National Science Foundation High Performance Computing and Communication program, Grant No. DMS-9218166.

[1]S. E. Holt, J. R. Koseff, and J. H. Ferziger, ''A numerical study of the evolution and structure of homogeneous stably stratified sheared turbulence,'' J. Fluid Mech. **237**, 499 (1992).
[2]E. C. Itsweire, J. R. Koseff, D. A. Briggs, and J. H. Ferziger, ''Turbulence in stratified shear flows: Implications for interpreting shear-induced mixing in the ocean,'' J. Phys. Oceanogr. **28**, 1508 (1993).
[3]K. B. Winters, P. N. Lombard, J. J. Riley, and E. A. D'Asaro, ''Available potential energy and mixing in density-stratified fluids,'' J. Fluid Mech. **289**, 115 (1995).
[4]Y. Noh and H. J. S. Fernando, ''Onset of stratification in a mixed layer subjected to a stabilizing buoyancy flux,'' J. Fluid Mech. **304**, 27 (1995).
[5]J. M. Redondo, M. A. Sanchez, and I. R. Cantalapiedra, ''Turbulent mechanisms in stratified fluids,'' Dyn. Atmos. Oceans **24**, 107 (1996).
[6]D. A. Briggs, J. H. Ferziger, J. R. Koseff, and S. G. Monismith, ''Turbulent mixing in a shear-free stably stratified two-layer fluid,'' J. Fluid Mech. **254**, 175 (1998).
[7]E. C. Itsweire, ''Measurements of vertical overturns in a stably turbulent flow,'' Phys. Fluids **27**, 764 (1984).
[8]M. C. Gregg, ''Diapycnal mixing in the thermocline: A review,'' J. Geophys. Res. **92**, 5249 (1987).
[9]G. N. Ivey and J. Imberger, ''On the nature of turbulence in a stratified fluid. Part I: The energetics of mixing,'' J. Phys. Oceanogr. **21**, 650 (1991).
[10]J. N. Moum, ''Energy-containing scales of turbulence in the ocean thermocline,'' J. Geophys. Res. **101**, 14 095 (1996).
[11]T. H. Ellison, ''Turbulent transport of heat and momentum from an infinite rough plane,'' J. Fluid Mech. **2**, 456 (1957).
[12]S. A. Thorpe, ''Turbulence and mixing in a Scottish loch,'' Proc. R. Soc. London, Ser. A **286**, 125 (1977).
[13]T. M. Dillon, ''Vertical overturns: A comparison of Thorpe and Ozmidov length scales,'' J. Geophys. Res. **87**, 9601 (1982).
[14]W. D. Smyth and J. N. Moum, ''Length scales of turbulence in stably stratified mixing layer,'' Phys. Fluids **12**, 1327 (2000).
[15]W. R. Crawford, ''A comparison of length scales and decay times of turbulence in stably stratified flows,'' J. Phys. Oceanogr. **26**, 1847 (1986).
[16]J. E. Broadwell and M. G. Mungal, ''Large-scale structures and molecular mixing,'' Phys. Fluids A **3**, 1193 (1991).
[17]H. Aref and S. W. Jones, ''Enhanced separation of diffusing particles by chaotic advection,'' Phys. Fluids A **1**, 470 (1989).
[18]C. R. Rehmann, ''Effects of stratification and molecular diffusivity on the mixing efficiency of decaying grid turbulence,'' Ph.D. thesis, Stanford University, 1995.
[19]H. J. S. Fernando, ''Turbulent mixing in stratified fluids,'' Annu. Rev. Fluid Mech. **23**, 455 (1991).
[20]H. J. S. Fernando and J. C. R. Hunt, ''Some aspects of turbulence and mixing in stably stratified layers,'' Dyn. Atmos. Oceans **23**, 35 (1996).
[21]E. C. Itsweire and K. N. Helland, ''Spectra and energy transfer in stably stratified turbulence,'' J. Fluid Mech. **204**, 479 (1989).
[22]Y. Noh and H. J. S. Fernando, ''The role of molecular diffusion in the deepening of the mixed layer,'' Dyn. Atmos. Oceans **17**, 187 (1993).
[23]I. A. Hannoun and E. J. List, ''Turbulent mixing at a shear-free density interface,'' J. Fluid Mech. **189**, 211 (1988).
[24]R. E. Breidenthal, ''Entrainment at thin stratified interfaces: the effects of Schmidt, Richardson, and Reynolds numbers,'' Phys. Fluids A **4**, 2141 (1992).
[25]E. N. Lorenz, ''Available potential energy and the maintenance of the general circulation,'' Tellus **7**, 157 (1955).
[26]T. M. Dillon and M. M. Park, ''The available potential energy of overturns as an indicator of mixing in the seasonal thermocline,'' J. Geophys. Res. **92**, 5345 (1987).
[27]A. H. Oort, S. C. Ascher, S. Levitus, and J. P. Peixóto, ''New estimates of the available potential energy in the world ocean,'' J. Geophys. Res. **94**, 3187 (1989).
[28]R. X. Huang, ''Mixing and available potential energy in a Boussinesq ocean,'' J. Phys. Oceanogr. **28**, 669 (1998).
[29]M. Hortmann, M. Perić, and G. Scheuerer, ''Finite volume multigrid prediction of natural convection: bench-mark solutions,'' Int. J. Numer. Methods Fluids **11**, 189 (1990).
[30]U. Ghia, K. N. Ghia, and C. T. Shin, ''High-Re solutions for incompressible flow using the Navier-Stokes equations and a multigrid method,'' J. Comput. Phys. **48**, 387 (1982).
[31]J. H. Ferziger and M. Perić, *Computational Methods for Fluid Dynamics* (Springer-Verlag, Berlin Heidelberg, 1996).
[32]S. B. Pope, ''Pdf methods for turbulent reactive flows,'' Prog. Energy Combust. Sci. **11**, 119 (1985).
[33]D. C. Stillinger, K. N. Helland, and C. W. Van Atta, ''Experiments on the transition of homogeneous turbulence to internal waves in a stratified fluid,'' J. Fluid Mech. **131**, 91 (1983).
[34]J. J. Rohr, E. C. Itsweire, K. N. Helland, and C. W. Van Atta, ''Growth and decay of turbulence in a stably stratified shear flow,'' J. Fluid Mech. **195**, 77 (1988).
[35]S. P. S. Piccirillo and C. W. Van Atta, ''The evolution of a uniformly sheared thermally stratified turbulent flow,'' J. Fluid Mech. **334**, 61 (1997).
[36]F. G. Jacobitz, S. Sarkar, and C. W. Van Atta, ''Direct numerical simulations of the turbulence evolution in a uniformly sheared and stably stratified flow,'' J. Fluid Mech. **342**, 231 (1997).
[37]L. H. Shih, J. R. Koseff, J. H. Ferziger, and C. R. Rehmann, ''Scaling and parameterization of stratified homogeneous turbulent shear flow,'' J. Fluid Mech. **412**, 1 (2000).
[38]R. S. Rogallo, ''Numerical experiments in homogeneous turbulence,'' NASA Tech. Memo. 81315, 1981.
[39]J. H. Lienhard V and C. W. Van Atta, ''The decay of turbulence in thermally stratified flow,'' J. Fluid Mech. **210**, 57 (1990).
[40]H. Yamazaki, ''Stratified turbulence near a critical dissipation rate,'' J. Phys. Oceanogr. **20**, 1583 (1990).
[41]C. H. Gibson, ''Fossil turbulence and intermittency in sampling oceanic mixing processes,'' J. Geophys. Res. **92**, 5383 (1987).